



HAL
open science

Simplified green-emitting single-layer phosphorescent organic light-emitting diodes with an external quantum efficiency > 22%

Fabien Lucas, Clément Brouillac, Sadiara Fall, Nicolas Zimmerman, Denis Tondelier, Bernard Geffroy, Nicolas Leclerc, Thomas Heiser, Christophe Lebreton, Emmanuel Jacques, et al.

► To cite this version:

Fabien Lucas, Clément Brouillac, Sadiara Fall, Nicolas Zimmerman, Denis Tondelier, et al.. Simplified green-emitting single-layer phosphorescent organic light-emitting diodes with an external quantum efficiency > 22%. *Chemistry of Materials*, 2022, 34 (18), pp.8345-8355. 10.1021/acs.chemmater.2c01909 . cea-03781036

HAL Id: cea-03781036

<https://cea.hal.science/cea-03781036>

Submitted on 20 Sep 2022

HAL is a multi-disciplinary open access archive for the deposit and dissemination of scientific research documents, whether they are published or not. The documents may come from teaching and research institutions in France or abroad, or from public or private research centers.

L'archive ouverte pluridisciplinaire **HAL**, est destinée au dépôt et à la diffusion de documents scientifiques de niveau recherche, publiés ou non, émanant des établissements d'enseignement et de recherche français ou étrangers, des laboratoires publics ou privés.

Simplified green-emitting single-layer phosphorescent organic light-emitting diodes with an external quantum efficiency > 22 %

Fabien Lucas,^{a*} Clément Brouillac,^b Sadiara Fall,^c Nicolas Zimmerman,^c Denis Tondelier,^a Bernard Geffroy,^{ad} Nicolas Leclerc,^e Thomas Heiser,^c Christophe Lebreton,^f Emmanuel Jacques,^f Cassandre Quinton,^b Joëlle Rault-Berthelot^b and Cyril Poriel^{b*}

^a LPICM, UMR CNRS 7647, Ecole Polytechnique, Institut Polytechnique de Paris, route de Saclay, 91128 Palaiseau, France

^b Univ Rennes, CNRS, ISCR-UMR CNRS 6226, F-35000 Rennes, France

^c Laboratoire ICube, Université de Strasbourg, UMR CNRS 7357, 67087 Strasbourg, France

^d Université Paris-Saclay, CEA, CNRS, NIMBE, LICSEN, 91191, Gif-sur-Yvette, France

^e Institut de Chimie et Procédés pour l'Énergie, l'Environnement et la Santé (ICPEES), UMR CNRS 7515, 67087 Strasbourg, France.

^f Univ Rennes, CNRS, IETR-UMR 6164, F-35000 Rennes, France

*corresponding authors: Fabien.lucas@polytechnique.edu and Cyril.poriel@univ-rennes1.fr

Abstract

Nowadays, Phosphorescent Organic Light-Emitting Diodes (PhOLEDs) is a widespread technology, in which all the high-performance devices are constructed on a stack of different organic layers called multi-layer devices (ML-PhOLEDs). Thanks to these functional layers, the injection, the transport and the recombination of holes and electrons in the Emissive Layer (EML) are significantly improved allowing to reach high performances. In this technology, the ideal devices are the Single-Layer PhOLEDs (SL-PhOLEDs), with a very simple stack only constituted of the electrodes and the EML. These devices are simple, very easy to fabricate and can hence significantly decrease their costs. Nevertheless, removing the functional layers of an OLED drastically decreases the performances and there is, so far, only a few examples of high performances SL-PhOLEDs. Thus, in SL-PhOLEDs, the role of the functional layer should be done by the EML, which should allow an excellent injection, transport and recombination of holes and electrons. In this work, thanks to a rational molecular design of the EML, we report a green emitting SL-PhOLED displaying a very high external quantum efficiency of 22.7 %. The EML of this device is constructed on the barely studied Ir(ppy)₂acac phosphor and a high efficiency host material possessing a Donor-*spiro*-Acceptor design. This performance is, to the best of our knowledge, the highest reported for SL-PhOLEDs (all colours considered). Through a structure/properties/device performance relationship study combining morphological (AFM), photophysical (time-resolved spectroscopy) and charge transport (SCLC) studies, we show that the EML presents all the required characteristics such as smooth surface, quick radiative deactivation and ambipolarity. In addition, the comparison with Ir(ppy)₃, the most famous green emitter used in PhOLEDs highlights the high potential of Ir(ppy)₂acac. The impact of the phosphorescent emitter on the ambipolarity of the charge transport is particularly evidenced.

Introduction:

Phosphorescent Organic Light Emitting Diodes (PhOLEDs) are the 2nd generation of OLEDs¹⁻⁵ (1st generation: fluorescent OLEDs⁶⁻⁸ / 3rd generation: thermally activated delayed fluorescence (TADF) OLEDs.⁹⁻¹²) PhOLEDs use a host-guest emissive layer (EML) in which the guest is an organometallic phosphorescent complex dispersed into an organic semiconductor (OSC), called host material. In a PhOLED, the maximal internal quantum efficiency (IQE_{max}) is of 100 % as both triplet (75 %) and singlet (25 %) excitons can be recovered on the contrary to fluorescent OLEDs (IQE_{max} of 25 %). Among the three generations of OLEDs, the PhOLED is the most mature device. The external quantum efficiencies (EQEs) of the most efficient PhOLEDs reported nowadays are very high, above 30 %.^{13, 14} Green- and red-emitting devices are already part of lighting displays available on the market.² This achievement has been possible thanks to the development of hundreds of host materials for the last 20 years.¹⁵⁻²⁰ Beside molecular engineering, the architecture of the device itself is of great importance to maximize the conversion of electric energy into luminous energy.²¹⁻²³ In this context, the most performant PhOLEDs to date are constructed on a multi-layer (ML) stack, which insures a good injection, transport and recombination of holes and electrons in the EML.^{13, 14, 23-26} Nevertheless, these devices remain complicated and simplifying the OLED technology is an important goal to decrease the production cost and the environmental footprint. One way to reduce these two main drawbacks is to use single-layer PhOLEDs (SL-PhOLEDs), which are the simplest possible OLED.¹⁵ In this kind of simplified architecture, the intermediate functional layers are removed and only the EML remains. Thus, in SL-PhOLEDs, the host material is more than ever the cornerstone of this simplified technology, as it should play the role of all the functional layers of ML-PhOLEDs. In such a material, several properties must be gathered: (i) a triplet state energy (E_T) higher than that of the phosphorescent emitter to confine the triplet excitons within the latter and allowing its single emission, (ii) high and equilibrated mobilities of electrons and holes (ambipolar character) to maximise excitons recombination within the centre of the EML and avoid leaks through the electrodes, (iii) HOMO and LUMO levels aligned with the Fermi level of the anode and the cathode to maximise holes and electrons injection respectively and (iv) good thermal and morphological stabilities to extend the OLED lifetimes.

Based on a *D-spiro-A* molecular design,²⁷⁻³⁷ we developed, in this work, a very high-efficiency bipolar host for green SL-PhOLEDs namely spiroquinolinophenothiazine-2-diphenylphosphine oxide-fluorene (**SQPTZ-2-FPOPh₂**) built on the combination of an electron-rich quinolinophenothiazine (QPTZ) fragment and an electron-deficient diphenylphosphine oxide-fluorene fragment (FPOPh₂). The QPTZ fragment is a building unit, which has shown, in recent years, promising features for electronic applications^{37, 38} and phosphine oxide is known to be a high efficiency electron-accepting unit.^{15, 39} The present bipolar host possesses all the above-mentioned required properties apart from the ambipolar character. An important finding in this work is indeed connected to the fact that we notice that using this **SQPTZ-2-FPOPh₂** host, ambipolarity can be achieved thanks to the

Figure 1. Cyclic voltammetry in reduction (left, DMF + Bu₄NPF₆ 0.1 M, sweep-rate 100 mV.s⁻¹) and in oxidation (middle, CH₂Cl₂ + Bu₄NPF₆ 0.2 M, sweep-rate 100 mV.s⁻¹) and emission spectrum at 77 K (2-MeTHF) of **SQPTZ-2-FPOPh₂**. From left to right inserted images are LUMO and HOMO electronic densities and spin density distribution of the first triplet state (TD-DFT B3LYP/6-311+G(d,p)).

In reduction, a reversible wave displaying a maximum at -2.23 V is detected. This wave is assigned to the reduction of the fluorene/phosphine oxide unit (Figure 1, left), giving a LUMO energy level of -2.31 eV. Thus, thanks to the *spiro* carbon, the electron-donating fragment and the electron-accepting fragment are spatially separated, which leads to a HOMO fully driven by the donor part and a LUMO fully driven by the acceptor part, according to TD-DFT calculations (see SI for details). In addition, electrochemical studies reveal that both first oxidation and reduction waves are reversible, showing the capability of **SQPTZ-2-FPOPh₂** to transport both type of charges, which is a key feature in simplified PhOLEDs. Finally, the electrochemical gap (ΔE_{el}) is relatively small, measured at 2.89 eV, with HOMO/LUMO energy levels (-5.20/-2.31 eV), in accordance with those of Ir(ppy)₂acac²⁸ (-5.06/-2.20 eV), see Figure 2. All these characteristics are of great interest for the SL device applications targeted herein particularly for the injection of charges.

The emission spectrum of **SQPTZ-2-FPOPh₂**, measured at 77K, reveals a first phosphorescent band at 441 nm, translating a high first triplet state energy level E_T of 2.81 eV (Figure 1, right) with a lifetime of 3.73 s (see Figure S9). The triplet spin density distribution (SDD) calculated by TD-DFT (B3LYP/6-311+G(d, p), Figure 1, right), displays that this first triplet state is centred on the fluorene backbone with no contribution of the QPTZ fragment and a very small one for the diphenylphosphine oxide fragment.

Finally, **SQPTZ-2-FPOPh₂** displays a very high decomposition (T_d =396°C) and glass transition (T_g= 150°C) temperatures (Figures S1-2), which are key properties for stability. Thus, thanks to the rigid *spiro* carbon bridge and the bulky diphenylphosphine oxide unit, the physical properties of **SQPTZ-2-FPOPh₂** appear to be excellent and in accordance with an optoelectronic application.

It is now interesting to compare the electronic and physical properties of **SQPTZ-2-FPOPh₂** with that of its analogue possessing two phosphine oxides attached at C2 and C7 (named **SQPTZ-2,7-FPOPh₂** see molecular structure in ref ⁴¹). Thus, the removal of one phosphine oxide in **SQPTZ-2-FPOPh₂** increases the electronic density on the fluorene,

increasing in turn the LUMO energy level (-2.60 vs -2.31 eV). This feature is directly linked to the electron withdrawing capability of the phosphine oxides. The HOMO energy level is also slightly increased in **SQPTZ-2-FPOPh₂** (-5.25 vs -5.20 eV) translating the connection between the two spiro connected fragment. The E_T is also significantly impacted by the removal of one phosphine oxide and increases from 2.76 eV in **SQPTZ-2,7-FPOPh₂** to 2.81 eV in **SQPTZ-2-FPOPh₂**. As the E_T is fully driven by the fluorene unit (and as the phosphorus atom does not completely break the conjugation), the presence of only one phosphine oxide unit increases the E_T . It should nevertheless be noted that the presence of the two phosphine oxides in **SQPTZ-2,7-FPOPh₂** improves both the T_g and the T_d compare to **SQPTZ-2-FPOPh₂**.

In the light of these promising properties, **SQPTZ-2-FPOPh₂** has been incorporated as host in green SL-PhOLEDs. Two different green phosphorescent emitters have been used in this study: the flagship Ir(ppy)₃ and Ir(ppy)₂acac. The former has been widely used in both ML- and SL-PhOLEDs with EQEs higher than 30 and 20 % respectively.^{13-15, 42} The later has been rarely used in ML-PhOLEDs⁴³ and even less in SL-PhOLEDs.⁴¹ Indeed, in SL-PhOLEDs, only three examples have been reported to date with Ir(ppy)₂acac and these devices all display low EQEs below 12 %.^{41, 44, 45} However, this phosphor displays interesting characteristics such as a narrower emission band than that of Ir(ppy)₃ with full width at half maxima (FWHM) of 64 nm against 68 nm, respectively. CIE coordinates (x;y) of Ir(ppy)₂acac complex are (0.34;0.63) and that of Ir(ppy)₃ are (0.31;0.63) which makes the former a greener emitter. Thus, to improve the diversity of green emitting phosphors in PhOLEDs, investigating new iridium complexes is particularly important and even more when display applications are targeted considering that the colour rendering is an important feature.

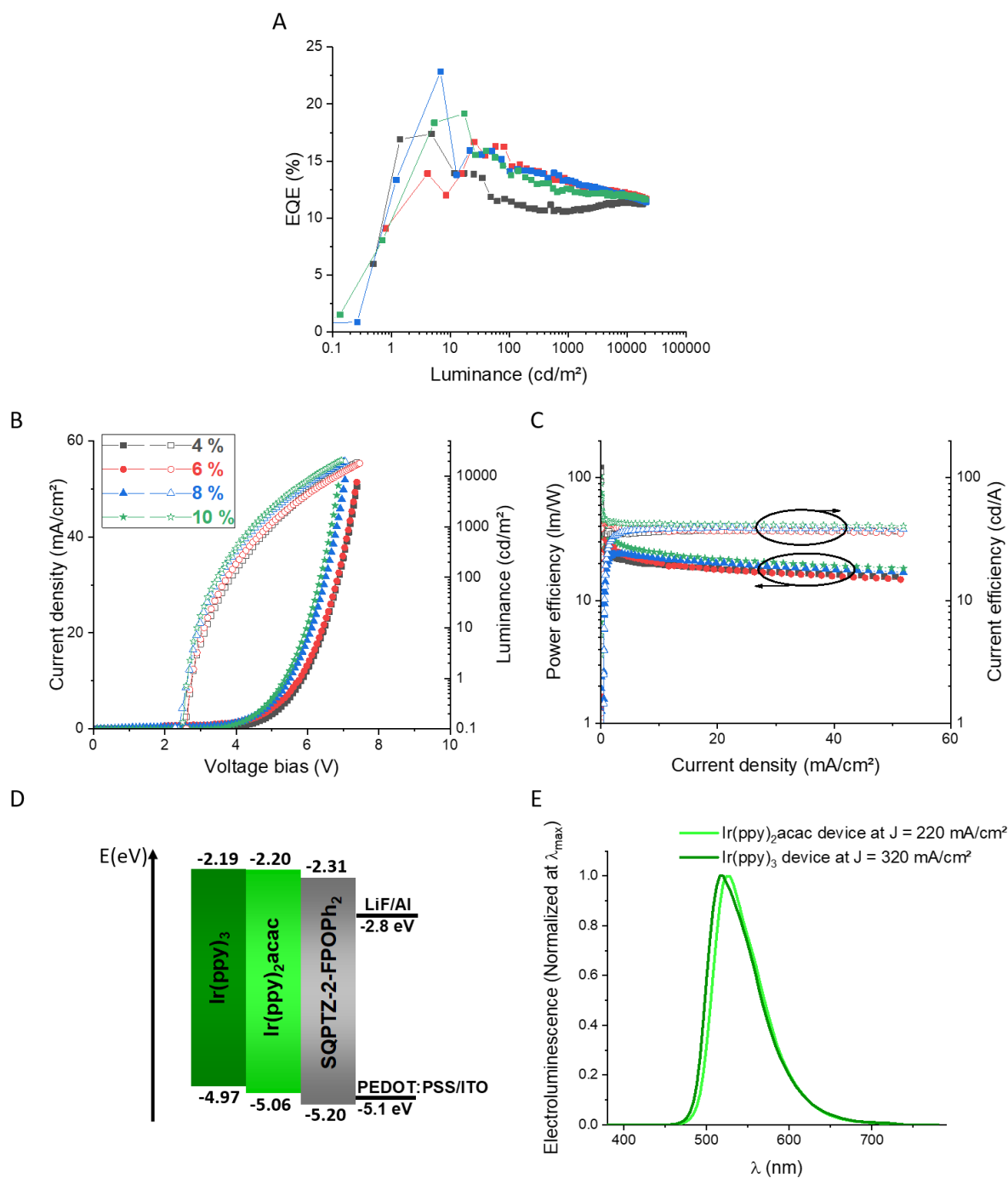


Figure 2. SL-PhOLEDs characteristics with **SQPTZ-2-FPOPh₂**:Ir(ppy)₂acac based EML at 4, 6, 8 and 10 % doping rate; (A) EQE (%) as a function of the luminance (cd/m²), (B) Current density (mA/cm²) and luminance (cd/m²) as a function of the bias voltage (V), (C) power efficiency (lm/W) and current efficiency (cd/A) as a function of the current density, (D) Simplified energetic diagram of the SL-PhOLEDs investigated and (E) electroluminescent spectra of SL-PhOLEDs incorporating **SQPTZ-2-FPOPh₂** as host either doped with 8% of Ir(ppy)₃ (dark green) or with 8% of Ir(ppy)₂acac (light green). The EML thickness of these devices is 100 nm.

The general SL-PhOLED structure used herein is : ITO/PEDOT:PSS (40 nm)/EML: **SQPTZ-2-FPOPh₂** + p % Ir(ppy)₂acac (100 nm)/LiF (1.2 nm)/Al (100 nm) with ITO/PEDOT:PSS as anode, LiF/Al as cathode and p is the doping rate. Before any device optimisation, classical conditions using found in SL-PhOLEDs have been first investigated, namely a doping rate (p) of 10 % and an EML thickness of 100 nm.^{28, 45-47} In these conditions, **SQPTZ-2-FPOPh₂** based SL-PhOLED exhibits a maximal external quantum efficiency (EQE_{max}) of 19.3 % at 0.01 mA/cm², a maximal luminance (L_{max}) of 50330 cd/m² at 190 mA/cm² and a low threshold voltage (V_{on}) of 2.7 V, Table 1. These performances are extremely high for simplified green SL-PhOLEDs and particularly for those incorporating Ir(ppy)₂acac. Before this work, the highest EQE recorded with this dopant in a SL-PhOLED was significantly lower, measured at 11.3 %. It should be nevertheless noted that the potential of Ir(ppy)₂acac (doped in CBP) has been previously highlighted in high efficiency ML PhOLEDs with EQE_{max} 20.7%.⁴³ In addition, one can note that the low V_{on} obtained at 0.1 cd/m² is slightly lower than the ΔE_{EI} of **SQPTZ-2-FPOPh₂** (see Figure 2), which indicates excellent charges injection in the host material. From a device engineering point of view, and particularly in a SL-PhOLED, the optimisation of the doping rate is important. However, when phosphorescent emitters are in play, quenching processes can happen such as triplet-triplet and triplet-polaron annihilations, which result in an important decrease of the performances, roll-off efficiency including, as the distance between guest molecules is decreasing.⁴⁸ So, an optimal doping rate must be found to prevent the quenching processes and maximise the transfers. Different doping rates p of 4, 6 and 8 % were then investigated. These devices yielded EQE_{max} of 17.2, 17.8 and 22.7 % respectively, Table 1. All these performances are very high and all significantly higher than the state-of-the-art performances of Ir(ppy)₂acac-based SL-PhOLEDs. This shows the high potential of **SQPTZ-2-FPOPh₂** as host in simplified SL-PhOLEDs. In particular, the EQE_{max} of 22.7 % obtained with a doping rate of 8 % is extremely high and, to the best of our knowledge, the highest reported in the literature for a simplified SL-PhOLED (whatever the emitter considered).⁴² Finally, note that the doping rate is less marked at 10 mA/cm², the EQEs are comprised between 11.3 and 11.9 %, see Table 1. This is an interesting finding as it indicates that even with a small amount of iridium complex very good performances can be obtained at high current density. From an industrialization point of view, this feature can result in lower production costs. The PhOLEDs performance at different luminance is found in Table 2. At 1000 cd.m⁻², the performance of the most efficient OLED is 13.3% (corresponding CE of 47.3 cd/A and LE of 32.9 lm/W)

In PhOLED technology, the phosphorescent dopant is, obviously, of key importance not only in term of efficiency but also in term of stability and colour rendering. However, only a few are commonly used. To find out about the impact of the phosphor in SL-PhOLED, a series of devices with the **SQPTZ-2-FPOPh₂** / Ir(ppy)₃ combination as EML have been fabricated, keeping the optimised doping rate of 8% and the same device architecture than that presented above. The corresponding SL-PhOLED yielded an EQE_{max} of 17.9 % at 0.01 mA/cm², a L_{max} of 51020 cd/m² at 320 mA/cm² and a V_{on} at 2.7 V (Table S5). There is hence a strong decrease of the EQE_{max}, from 22.7 % with Ir(ppy)₂acac to 17.9 % with Ir(ppy)₃, which

can only be imputed to the emitter. At 10 mA/cm², there is still a high difference of 3 % between the two phosphors (11.9 % for Ir(ppy)₂acac device vs 8.7 % for Ir(ppy)₃ device). The luminance, measured at the same current density (220 mA/cm²), is also significantly higher for Ir(ppy)₂acac than for Ir(ppy)₃: 50920 cd/m² and 40850 cd/m² respectively. The origin of the difference between these two sets of devices and the very high performances obtained with the Ir(ppy)₂acac based devices should then be unravelled.

Table 1 SL-PhOLED performances using **SQPTZ-2-FPOPh₂** as host and Ir(ppy)₂acac as phosphorescent dopant. Device architecture: ITO/PEDOT:PSS (40 nm)/host + p % dopant (100 nm)/LiF (1.2 nm)/Al (100 nm) where p is the doping rate.

p (%)	V _{on} (V)	EQE (%)	CE (cd/A)	PE (lm/W)	L (cd/m ²)	EQE (%)	CE (cd/A)	PE (lm/W)	L (cd/m ²)	CIE coordinates (x ; y)
		At 10 mA/cm ²				Max (at J (mA/cm ²))				At 10 mA/cm ²
4	2.8	11.3	26.2	36.0	4093	17.2 (0.01)	56.0 (0.01)	56.1 (0.01)	47910 (170)	0.32 ; 0.64
6	2.8	12.2	24.7	42.9	4100	17.8 (0.02)	65.2 (0.02)	63.1 (0.02)	47700 (200)	0.32 ; 0.64
8	2.7	11.9	20.2	42.6	3923	22.7 (0.01)	87.8 (0.01)	81.0 (0.01)	50920 (220)	0.32 ; 0.64
10	2.7	12.5	25.4	43.4	4430	19.3 (0.01)	71.6 (0.01)	67.1 (0.01)	50330 (190)	0.34 ; 0.63

Table 2 SL-PhOLED performances at 1, 100 and 1000 cd/m² with **SQPTZ-2-FPOPh₂**; Ir(ppy)₂acac, at 4, 6, 8 or 10% doping ratio. Device structure: ITO/PEDOT:PSS (40 nm)/host + dopant (100 nm)/LiF (1.2 nm)/Al (100 nm).

p (%)	EQE (%)	CE (cd/A)	PE (lm/W)	EQE (%)	CE (cd/A)	PE (lm/W)	EQE (%)	CE (cd/A)	PE (lm/W)
	At 1 cd/m ²			At 100 cd/m ²			At 1000 cd/m ²		
4	16.9	55.4	62.2	11.5	37.5	30.3	10.6	34.8	23.5
6	9.1	31.9	38.6	14.5	51.1	46.0	13.2	46.3	32.8
8	13.4	47.6	55.4	14.1	50.3	45.2	13.3	47.3	32.8
10	8.0	28.0	33.8	13.7	47.8	42.9	12.6	43.8	33.0

First, the morphology of the EML is known to have a great influence on the efficiency of an organic electronic device.^{49, 50} Thus, we have investigated the roughness of both EMLs by performing AFM studies, Figure 3. Samples presenting the same architecture as the corresponding SL-PhOLEDs, *i.e.* ITO/PEDOT:PSS (40nm)/EML (100nm) were prepared.

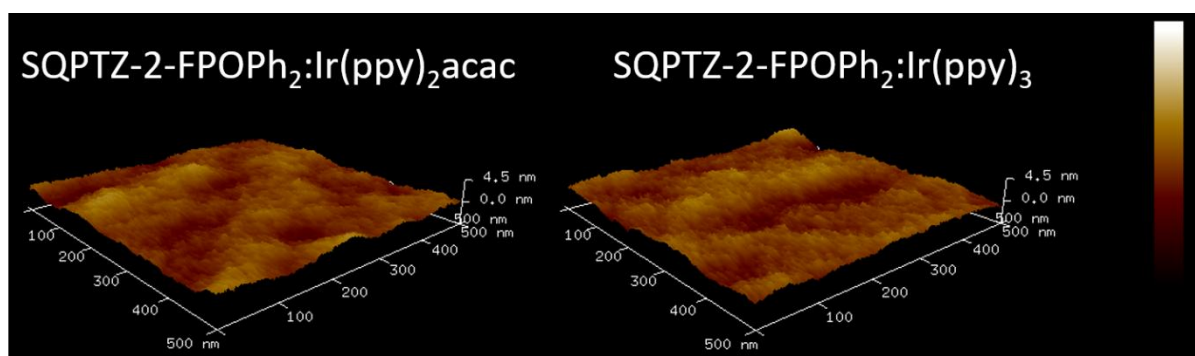


Figure 3 2D ($500 \times 500 \text{ nm}^2$) AFM images of (left) **SQPTZ-2-FPOPh₂ + 8 % Ir(ppy)₂acac** (100 nm) and (right) **SQPTZ-2-FPOPh₂ + 8 % Ir(ppy)₃** (100 nm) EMLs.

The film surface of the Ir(ppy)₂acac based EML presents a root mean surface roughness (R_q) of 0.549 nm while the one of Ir(ppy)₃ based EML is 0.557 nm. These two R_q are really close and show that the morphology of the EMLs are not impacted by the nature of the dopant. From this point of view, the extraction of light might follow the same path for both. These values also show that the quality of the interfaces with PEDOT:PSS is identical, which is in accordance with the V_{ON} , 2.7 V for both sets of devices. This is a very interesting feature as it shows that the good performances obtained with both dopants are undoubtedly linked to this macroscopic characteristic. Nevertheless, to unravel the origin of the different performances between the two emitters, molecular interactions between the host and the two dopants should be considered. Kim and co-workers have shown that the orientation of the emitting dipoles is crucial to maximise the extraction of light, resulting in an increase of the EQE_{max} .⁵¹ They have shown that the phosphorescent emitter Ir(ppy)₂acac has preferential horizontal-directed emitting dipoles when it is 8 % doped in the exciplex forming co-host TCTA:B3PYMPM (1:1). This orientation allows to enhance the light extraction. Similarly, Wu and co-workers have compared the performances of ML-PhOLEDs using either Ir(ppy)₃ or Ir(ppy)₂acac 8 % doped in CBP.⁵² They have shown that, while Ir(ppy)₃ has randomly oriented emitting dipoles in the EML, the preferentially horizontal-directed emitting dipoles of Ir(ppy)₂acac in the EML allow to increase the EQE of 2 to 3 %. In our study, we have observed the same improvement in term of EQE at 10 mA.cm^{-2} , going from 8.7 % for Ir(ppy)₃ device to 11.9 % for Ir(ppy)₂acac device. Thus, the very high efficiency obtained with Ir(ppy)₂acac-based EML can be due, at least partially, to a similar behaviour as that shown by Wu and co-workers, showing the potential of this phosphor in PhOLEDs.

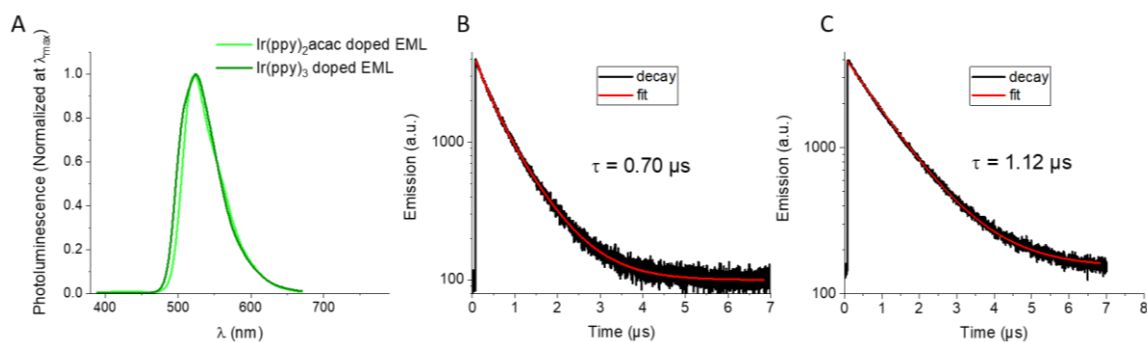


Figure 4 (A) Steady state photoluminescence spectra of the EML 8 % doped Ir(ppy)₂acac ($\lambda_{exc} = 366$ nm) or Ir(ppy)₃ ($\lambda_{exc} = 340$ nm) into **SQPTZ-2-FPOPh₂** and time resolved photoluminescence (B) of the EML 8 % doped with Ir(ppy)₂acac ($\lambda_{exc} = 310$ nm, $\lambda_{em} = 525$ nm) and (C) of the EML 8 % doped with Ir(ppy)₃ ($\lambda_{exc} = 310$ nm, $\lambda_{em} = 525$ nm). The thickness of the EMLs is 100 nm.

To get additional insights on excitons transfers and photophysical mechanisms, we have performed steady state and time resolved spectroscopy experiments of the EML 8 % doped either with Ir(ppy)₃ or Ir(ppy)₂acac, Figure 4. First of all, both EML present photoluminescence spectra matching with their corresponding electroluminescence spectra (Figure 2E and Figure 4A). This shows that excitons transfers from the host to the emitter are highly efficient and do not depend on the dopant used, highlighting the efficiency of the *D-spiro-A* molecular design. The radiative deactivation of the EML is also a very important data to insure an efficient emission and should also be considered. The Ir(ppy)₂acac-based EML exhibits a lifetime decay below 1 μs ($\tau = 0.70$ μs at $\lambda_{em} = 525$ nm) while the Ir(ppy)₃-based EML shows a longer lifetime decay with $\tau = 1.12$ μs at the same emission wavelength. Therefore, the lifetime of the Ir(ppy)₂acac-based EML is significantly reduced compared to that of Ir(ppy)₃. The quicker radiative deactivation of the triplet state of the Ir(ppy)₂acac complex can be related to the high efficiency reached due to a decrease of triplet-triplet annihilation.⁵³⁻⁵⁸ Note that the link between high PhOLED performance and short deactivation lifetime of the EML has been recently highlighted in high performance ML-PhOLEDs.⁵³

The charge transport within the EML should also be considered as a key feature to explain the high performance of the SL-PhOLEDs. In the field of SL-PhOLEDs, the ability of the host to transport both electrons and holes efficiently and as balanced as possible is an important property to maximise the formation of excitons preferably in the centre of the EML.¹⁵ So, **SQPTZ-2-FPOPh₂** has been incorporated in hole-only and electron-only space charge limited current (SCLC) devices to extract charge carriers mobilities (see SI for device architectures, fabrication processes and electrical characteristics). The hole (μ_h) and electron (μ_e) mobilities have been estimated at $5.1 \pm 2.1 \times 10^{-8}$ and $1.1 \pm 1.6 \times 10^{-4}$ cm².V⁻¹.s⁻¹, respectively. Thus, **SQPTZ-2-FPOPh₂** has a hole mobility 2000 times lower than its corresponding electron mobility. For a *spiro* compound, displaying a 3D shape, the electron mobility appears to be particularly high but the transport is not properly balanced, which is not in accordance with a very high SL-PhOLED performance. However, the impact of the iridium complex, present in

the EML, is not reflected by these data. The charge transport of the EML, including 8 % of Ir(ppy)₂acac, was thus precisely determined through characterization of SCLC devices and has provided hole and electron mobilities of $7.2 \pm 3.0 \times 10^{-7}$ and $7.6 \pm 2.3 \times 10^{-6} \text{ cm}^2 \cdot \text{V}^{-1} \cdot \text{s}^{-1}$. This leads to a μ_e/μ_h ratio of 11, close to unity. Surprisingly, we observed that the hole mobility is increased while the electron mobility is decreased compared to the neat host helping to reach a more balanced hole and electron transport. This balance of hole and electron flow within the EML appears as a central notion to insure an efficient charge recombination in the centre of the EML. The same experiments were conducted for the couple **SQPTZ-2-FPOPh₂**/Ir(ppy)₃ and provides values of $7.1 \pm 1.5 \times 10^{-8}$ and $1.1 \pm 2 \times 10^{-5} \text{ cm}^2 \cdot \text{V}^{-1} \cdot \text{s}^{-1}$. In this latter case, the μ_e/μ_h ratio (>140) is larger and less balanced than the Ir(ppy)₂acac based EML displays a more balance charge transport than Ir(ppy)₃ based EML. In the light of the importance of ambipolarity in SL-PhOLEDs, one can consider that the higher performances obtained for Ir(ppy)₂acac arises from this feature.

Finally, to ascertain the efficiency of the *D-Spiro-A* molecular design in the SL-PhOLED performance, Ir(ppy)₂acac-based SL-PhOLEDs using two commercially available host materials, 4,4'-bis(*N*-carbazolyl)-1,1'-biphenyl (CBP, HOMO/LUMO: -5.56/-2.09 eV, $E_T = 2.69$ eV) and 1,3-bis(*N*-carbazolyl)benzene (mCP, HOMO/LUMO: -5.64 / -1.90 eV, $E_T = 3.05$ eV), have been fabricated. These hosts are commonly found in literature in high performance devices.^{24, 59-62} For the purpose of this work and to keep consistency HOMO, LUMO and E_T levels of CBP and mCP have been measured in identical conditions than that used for **SQPTZ-2-FPOPh₂** (see SI Figures S14-15 and Table S5). The architecture of these benchmark devices is identical to those reported above and the different performance can then only be ascribed to the host. The performances recorded for both compounds appear to be very low with EQE_{max} of 1.3 % (CBP) and 2.6 % (mCP) measured at 10 mA/cm². V_{ON} are very high, 4.6 and 4.1 V, and L_{max} very low, 1487 cd/m² (at 70 mA/cm²) and 1213 cd/m² (at 50 mA/cm²) for CBP and mCP respectively (see Figures S14-15 and Table S5). We attribute the poor performances of these two matrices to a poor electron transport in the host material as both of these matrices are only made on electron-donating carbazole moieties. This confirms the importance of the ambipolarity of the charge transport to achieve high efficiency SL-PhOLEDs.

To conclude, we report a high efficiency EML for SL-PhOLED, namely Ir(ppy)₂acac as emitter and **SQPTZ-2-FPOPh₂** as host material. Constructed on a *D-spiro-A* design, **SQPTZ-2-FPOPh₂** gathers all required photophysical, electronic, thermal and morphological properties for high performance simplified green-emitting SL-PhOLEDs. One of the peculiarities of this work lies in the use of the barely studied Ir(ppy)₂acac emitter, which appears significantly, in combination with our host molecule, more efficient than the well-known Ir(ppy)₃ emitter. An extremely high EQE of 22.7 % (CE = 87.8 cd/A, PE = 81.0 lm/W, $V_{on} = 2.7$ V and $L_{max} = 50920$ cd/m²) was reached with CIE coordinates of 0.32;0.64 at 10 mA/cm², which is, to the best of our knowledge, the highest reported for this technology of simplified OLEDs (for all colour). Beside the good alignment of LUMO levels of the host material and the dopant, the high

performance arises from the excellent balance of the charge carriers within the EML, rapid radiative deactivation processes and smooth roughness surface. These characteristics appear to be more efficient to reach high performance than those of Ir(ppy)₃, the flagship green emitter in PhOLED technology. These performances are also significantly higher than those of well-known commercially available host matrices, CBP and mCP, demonstrating the efficiency of the molecular design strategy. This work shows that the performance of SL-PhOLEDs are closer and closer to those of ML-PhOLEDs and bridges the gap between these two technologies.

Conflicts of interest

There are no conflicts to declare.

Acknowledgements

The author highly thank the Agence Nationale de la Recherche (Project *Spiroquest* N°19-CE05-0024) for PhD and post-doctoral grants (CB and FL respectively). The ADEME (*Ecoelec* Project) is also warmly acknowledged for PhD grant (CB). We also thank the CRMPO (Rennes) for mass analyses and GENCI (Project N°AD0100805032R1) for computing time.

Supporting Information

General experimental methods, synthetic procedures, compounds characterizations, copy of mass and NMR spectra and thermal, photophysical, electrochemical, computational and devices data are provided.

General experimental methods⁴¹

Synthesis

All manipulations of oxygen and moisture-sensitive materials were conducted with a standard Schlenk technique. All glassware was kept in an oven at a temperature of 80°C. Argon atmosphere was generated by three repetitive cycles of vacuum/Argon using a schlenk ramp. Commercially available reagents and solvents were used without further purification other than those detailed below. THF was obtained through a PURE SOLV™ solvent purification system. Light petroleum refers to the fraction with bp 40-60°C. Analytical thin layer chromatography was carried out using aluminum backed plates coated with Merck Kieselgel 60 GF254 and visualized under UV light (at 254 and 360 nm). Flash chromatography was carried out using Teledyne Isco CombiFlash® Rf 400 (UV detection 200-360 nm), over standard silica cartridges (Redisep® Isco or Puriflash® columns Interchim). ¹H and ¹³C NMR spectra were recorded using Bruker 300 MHz instruments (¹H frequency, corresponding ¹³C frequency: 75 MHz); chemical shifts were recorded in ppm and J values in Hz. The residual signals for the NMR solvents used are 5.32 ppm (proton) and 53.84 ppm (carbon) for CD₂Cl₂.⁶³ In the ¹³C NMR spectra, signals corresponding to C, CH, CH₂ or CH₃ groups, assigned

from DEPT experiment, are noted. The following abbreviations have been used for the NMR assignment: s for singlet, d for doublet, t for triplet, q for quadruplet and m for multiplet. High resolution mass spectra were recorded at the Centre Régional de Mesures Physiques de l'Ouest (CRMPO-Rennes) on a Thermo Fisher Q-Exactive instrument or a Bruker MaXis 4G or a Bruker Ultraflex III.

Spectroscopic studies

Cyclohexane (spectroscopic grade, Acros) and 2-MeTHF (Anhydrous, >99 %, Sigma Aldrich) were used without further purification.

UV-visible spectra were recorded using an UV-Visible spectrophotometer SHIMADZU UV-1605. Molar extinction coefficients (ϵ) were calculated from the gradients extracted from the plots of absorbance vs concentration with five solutions of different concentrations for each sample.

$$A = \epsilon \times l \times C$$

Steady state and time resolved emission spectra were recorded with a HORIBA Scientific Fluoromax-4 equipped with a Xenon lamp. Triplet energy levels were calculated from the maximum of the first phosphorescence emission peak at 77 K. Conversion in electron-volt was obtained with the following formula: $E_T(eV) = \frac{hc}{\lambda}$ with $h = 6.62607 \times 10^{-34}$ J.s, $C = 2.99792 \times 10^{17}$ nm.s⁻¹ and $1 \text{ eV} = 1.60218 \times 10^{-19}$ J. This equation can be simplified as: $E_T(eV) = \frac{1239.84}{\lambda}$ with λ formulated in nm.

Low temperature (77 K) measurements were performed in 2-MeTHF which freezes as a transparent glassy matrix. Measurements were carried in a single block quartz tube containing the solution, which was placed in an oxford Optistat Cryostat cooled with liquid nitrogen.

Infrared spectra were recorded on a Bruker Vertex 70 using a diamond crystal MIRacle ATR (Pike).

Electrochemical studies

Electrochemical experiments were performed under argon atmosphere using a Pt disk electrode (diameter 1 mm). The counter electrode was a vitreous carbon rod. The reference electrode was either a silver wire in a 0.1 M AgNO₃ solution in CH₃CN for the studies in oxidation or a Silver wire coated by a thin film of AgI (silver(I)iodide) in a 0.1 M Bu₄NI solution in DMF for the studies in reduction. Ferrocene was added to the electrolyte solution at the end of a series of experiments. The ferrocene/ferrocenium (Fc/Fc⁺) couple served as internal standard. The three electrodes cell was connected to a potentiostat/galvanostat (Autolab/PGSTAT101) monitored with the Nova 2.1 Software. Activated Al₂O₃ was added in the electrolytic solution to remove excess moisture. For a further comparison of the electrochemical and optical properties, all potentials are referred to the SCE electrode that

was calibrated at -0.405 V vs. Fc/Fc^+ system. We estimated the electron affinity (EA) or lowest unoccupied molecular orbital (LUMO) and the ionization potential (IP) or highest occupied molecular orbital (HOMO) from the redox data. The LUMO level was calculated from the cyclic voltammetry in reduction as follow: $\text{LUMO (eV)} = -[\text{E}_{\text{onset}} (\text{vs SCE}) + 4.4]$. Similarly the HOMO level was calculated from the cyclic voltammetry in oxydation as follow: $\text{HOMO (eV)} = -[\text{E}_{\text{onset}} (\text{vs SCE}) + 4.4]$ based on an SCE energy level of 4.4 eV relative to the vacuum. The electrochemical gap was calculated from: $\Delta E^{\text{el}} = |\text{HOMO-LUMO}|$ (in eV).

Molecular modelling

Full geometry optimization of the ground state (S_0) and vibrational frequency calculation were performed with Density Functional Theory (DFT)^{64, 65} using the hybrid Becke-3 parameter exchange functional⁶⁶⁻⁶⁸ and the Lee-Yang-Parr non-local correlation functional⁶⁹ (B3LYP) implemented in the Gaussian 16 program suite,⁷⁰ using the 6-31G(d) basis set and the default convergence criterion implemented in the program. All stationary points were characterized as minima by analytical frequency calculations. Optical transition diagrams were obtained through TD-DFT calculations performed using the B3LYP functionals and the 6-311+G(d,p) basis set from the optimized geometry of S_0 . Geometry optimization of the first excited triplet state (T1) was performed using Time-Dependent Density Functional Theory (TD-DFT) calculations using the B3LYP functional and the 6-311+G(d,p) basis set. Spin density (SD) representation was obtained through TD-DFT calculations performed using the B3LYP functional and the extended 6-311+G(d,p) basis set and a triplet spin on the previously optimized geometry of T1. T1 to S_0 energy transition (ET) was calculated from the difference between the total energy of the molecule in its respective excited triplet state (found trough TD- DFT, B3LYP 6-311+G(d,p)) and its ground singlet state (found through DFT, B3LYP 6-311+G(d,p)) in their optimized geometries.

Calculations were carried out on the OCCIGEN calculator of the Centre Informatique National de l'Enseignement Supérieur (CINES (Montpellier) under project N° 2021-A0100805032).

Thermal analysis

Thermal Gravimetric Analysis (TGA) was carried out by using a Mettler-Toledo TGA-DSC-1 apparatus. TGA curved were measured at $10^\circ\text{C}/\text{min}$ from 30°C to 1000°C under a nitrogen flux. Differential Scanning Calorimetry (DSC) was carried out by using a NETZSCH DSC 200 F3 instrument equipped with an intracooler DSC traces were measured at $10^\circ\text{C}/\text{min}$, 2 heating/cooling cycles were successively carried out under a nitrogen flux.

Devices fabrication and characterization

- Single layer phosphorescent organic light emitting diodes (SL-PhOLEDs)

The structure of the SL devices is the following: ITO/PEDOT:PSS (40 nm)/Emissive layer *host:guest p %* (100 nm)/LiF (1.2 nm)/Al (100 nm). In this devices, ITO/PEDOT:PSS (poly(3,4-ethylenedioxythiophene)-poly(styrenesulfonate)) is used as the anode and a thin film of lithium fluoride covered with aluminum is the cathode. The devices have been fabricated onto patterned ITO coated glass substrates from XinYan Tech (thickness: 100 nm and sheet resistance: less of 20 W/m). The organic materials are deposited onto the ITO anode by sublimation under high vacuum ($< 10^{-6}$ Torr) at a rate of 0.2 – 0.3 nm/s. The entire device is fabricated in the same run without breaking the vacuum. In this study, the thicknesses of the different organic layers were kept constant for all the devices. The active area of the devices defined by the overlap of the ITO anode and the metallic cathode was 0.3 cm². The current-voltage-luminance (I-V-L) characteristics of the devices were measured with a regulated power supply (Laboratory Power Supply EA-PS 3032-10B) combined with a multimeter and a 1 cm² area silicon calibrated photodiode (Hamamatsu). The spectral emission was recorded with a SpectraScan PR650 spectrophotometer. All the measurements were performed at room temperature and at ambient atmosphere with no further encapsulation of devices.

- Space-charged limited current (SCLC) devices

Fabrication of hole-only space-charge limited current (SCLC) devices: Indium-tin oxide (ITO) coated glass was used as a substrate. A sequential cleaning of the substrates in soap water, distilled water, acetone and isopropanol (15 min for each step) using ultrasonic bath was performed. A thin, highly conductive poly(ethylenedioxythiophene):polystyrene sulfonate (PEDOT:PSS) layer was spin-coated onto pre-cleaned ITO and used as a bottom electrode. Then samples were thermally annealed at 120°C for 15 min. The active layer was co-evaporated under high vacuum ($< 10^{-6}$ Torr) at a rate of 0.2 – 0.3 nm/s SCLC devices were completed by sequential thermal evaporation of MoO₃ (7nm) and Ag (250 nm) layers.

Fabrication of electron-only space-charge limited current (SCLC) devices: Identical ITO substrates and cleaning conditions were applied as for hole-only samples (see above). A thin ZnO layer (20-25 nm) was spin-coated onto pre-cleaned ITO and thermally annealed at 110°C for 10 min and used as a bottom contact. The active layer was deposited as previously for hole-only SCLC devices, devices were completed by a sequential evaporation of Ca (20 nm) and Al (300 nm) as a top contact.

SCLC diode current-voltage characteristics were measured, inside the glove-box, using Keithley semiconductor characterization system 4200. The active-layer thicknesses were measured after SCLC characterization using a profilometer.

Atomic force microscopy measurement

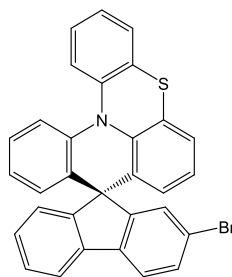
AFM images were recorded on the Bruker Multimode 8 using PeakForce Tapping with a resolution of 512x512 pixels on a 500nmx500nm surface. Scan rate has been set at 1Hz. Each scan line in the image was scanned from left to right (trace) and from right to left (retrace). The observed topographic features were verified for their consistency between trace and retrace images. Amplitude setpoint was set to 2.81mV and the drive amplitude was set to

10.38mV. Roughness has been extracted from these images using Nano Scope Analysis 1.8 after a clean image treatment.

Synthetic procedures

QPTZ-Br was synthesized as previously described.⁴¹ The following procedures follow a previous report and are restated here for clarity.⁴¹

2-Bromospiro[fluorene-9,9'-quinolino[3,2,1-kl]phenothiazine] [**SQPT-2-FBr**]



1st step: The solution of **QPTZ-Br** (1.64 g, 4.63 mmol, 1.2 eq) in dry THF (50 mL) under argon was cooled to -78°C. *n*-BuLi (2.50 M in hexanes, 1.85 mL, 4.63 mmol, 1.2 eq) was then added dropwise and the resulting mixture was stirred for 30 min. 2-Bromofluorenone (1.00 g, 3.86 mmol, 1.0 eq) dissolved in dry THF (15 mL) at -78°C was added dropwise to the reaction mixture and stirred for 30 additional minutes. Then, the reaction was allowed to warm up to room temperature under stirring overnight. Solvent was removed under reduced pressure and the crude product was dried under vacuum at 60°C for 2 hours.

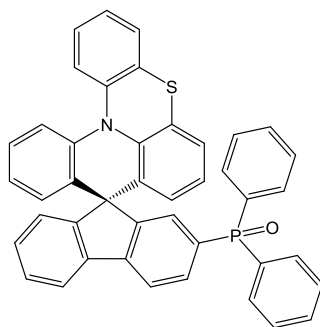
2nd step: Without further purification, the crude mixture was dissolved in acetic acid (50 mL) and hydrochloric acid (5 mL) was added under stirring. The reaction mixture was refluxed for 5 hours under stirring.

After cooling to room temperature, water was added to the reaction mixture. The precipitate was filtered off and then dissolved in CH₂Cl₂. The organic layer was washed with water and dried over MgSO₄. Solvent was then removed under reduced pressure. A hot saturated solution of the crude in CHCl₃ was prepared and the product was precipitated by adding MeOH. This was repeated several times. Product was finally dried under vacuum at 40°C overnight.

After precipitation, from a mixture of CHCl₃/MeOH, a white solid was obtained (1.74 g, yield 87 %). ¹H NMR (300 MHz, CD₂Cl₂) δ 7.80 (d, J = 8.1 Hz, 1H), 7.75 – 7.66 (m, 2H), 7.56 – 7.47 (m, 2H), 7.44 – 7.35 (m, 2H), 7.31 – 6.97 (m, 7H), 6.91 – 6.76 (m, 2H), 6.56 (dd, J = 7.9, 1.5 Hz, 1H), 6.37 (dd, J = 7.8, 1.4 Hz, 1H) ppm. ¹³C NMR (75 MHz, CD₂Cl₂): δ 154.3 (C), 153.1 (C), 143.5 (C), 142.2 (C), 139.6 (2C), 136.7 (C), 132.5 (C), 132.3 (CH), 130.6 (CH), 130.4 (C), 129.2 (CH), 129.1 (CH), 128.5 (CH), 128.3 (CH), 128.2 (CH), 127.5 (CH), 127.4 (C), 126.6 (CH), 125.4 (CH), 125.2 (CH), 125.0 (C), 124.8 (CH), 124.5 (CH), 124.3 (CH), 122.5 (C), 122.2 (CH), 121.1 (CH), 120.7 (CH), 119.4 (CH), 57.9 (C) ppm. IR (ATR, platinum): 3062, 1916, 1771, 1703, 1653,

1590, 1580, 1566, 1506, 1489, 1478, 1455, 1436, 1404, 1321, 1302, 1289, 1271, 1255, 1231, 1215, 1190, 1160, 1131, 1123, 1111, 1082, 1063, 1035, 1006, 979, 962, 949, 934, 919, 885, 872, 853, 820, 789, 773, 745, 721, 696, 679, 654, 640, 622, 576, 550, 528, 507, 488, 472, 443, 433, 423 cm^{-1} . HRMS (MALDI, DCTB): Found $[\text{M}^+]$ 515.033 for $\text{C}_{31}\text{H}_{18}\text{BrNS}$ required 515.03378. m.p.: 262 °C

Diphenyl(spiro[fluorene-9,9'-quinolino[3,2,1-kl]phenothiazin]-2-yl)phosphine oxide [**SQPTZ-2-FPOP₂**]



1st step: **SQPTZ-2-FBr** (0.500 g, 0.97 mmol, 1.0 eq) was dissolved in dry THF (45 mL) under argon. The reaction mixture was then cooled to -78°C and *n*-BuLi (2.50 M in hexanes, 0.58 mL, 1.45 mmol, 1.5 eq) was added dropwise. The reaction mixture was stirred for 2 hours at -78°C. Chlorodiphenylphosphine (0.27 mL, 1.45 mmol, 1.5 eq) was then added and the mixture was stirred for 2 additional hours at -78°C. The reaction mixture was finally allowed to warm up to room temperature under stirring overnight. The reaction mixture was quenched with few drops of absolute ethanol and concentrated under reduced pressure. The crude product was dissolved in CH_2Cl_2 . The organic layer was washed with water, brine, dried over MgSO_4 and filtered. Solvent was removed under reduced pressure and dried under vacuum at 60°C for 5 hours.

2nd step: Without any further purification, the crude mixture was dissolved in CH_2Cl_2 (50 mL) and H_2O_2 (5 mL, 35 wt. % in water) was added to the mixture which was stirred overnight at room temperature. The organic layer was washed several times with water and dried over MgSO_4 . Solvent was then evaporated under reduced pressure and the crude product was purified with flash chromatography on silica gel [column condition: silica cartridge (40 g); solid deposit on Celite®; λ detection: (254 nm, 280 nm); gradient $\text{CH}_2\text{Cl}_2/\text{CH}_3\text{OH}$ from 100 % to 95 % in 40 min at 40 mL/min]. The *title compound* was obtained as a white solid 0.311 g 50 % ^1H NMR (300 MHz, CD_2Cl_2) δ 8.01 (dd, $J = 7.8, 2.4$ Hz, 1H), 7.80 (d, $J = 7.6$ Hz, 1H), 7.72 – 7.23 (m, 17H), 7.23 – 7.00 (m, 5H), 6.84 (t, $J = 7.6$ Hz, 1H), 6.77 (t, $J = 7.7$ Hz, 1H), 6.52 (dd, $J = 8.0, 1.5$ Hz, 1H), 6.36 – 6.28 (m, 1H) ppm. ^{13}C NMR (75 MHz, CD_2Cl_2) δ 155.0 (C), 151.0 (C), 146.7 (C), 143.3 (C), 139.7 (C), 139.5 (C), 136.5 (C), 134.3 (C), 134.1 (C), 133.2 (C), 132.9 (CH), 133.0 (CH), 132.6 (CH), 132.4 (CH), 131.2 (CH), 131.1 (CH), 130.4 (C), 130.1 (CH), 129.1 (CH), 129.0 (CH), 129.0 (CH), 128.5 (CH), 128.3 (CH), 128.2 (CH), 127.4 (C), 127.2 (CH), 126.5 (CH), 125.2 (CH), 125.1 (C), 125.0 (CH), 124.6 (CH), 124.4 (CH), 124.4 (CH), 121.9 (CH), 121.0 (CH),

120.8 (CH), 120.6 (CH), 119.4 (CH), 58.0 (C) ppm. ³¹P NMR (121 MHz, CD₂Cl₂) δ 27.4 ppm. IR (ATR, platinum): 3671, 3416, 3055, 1606, 1588, 1569, 1488, 1477, 1454, 1436, 1403, 1323, 1314, 1291, 1270, 1252, 1229, 1203, 1185, 1170, 1160, 1148, 1129, 1116, 1106, 1083, 1070, 1035, 1026, 998, 929, 918, 893, 869, 855, 834, 800, 782, 746, 722, 703, 695, 681, 668, 644, 621, 592, 555, 542, 517, 488, 465, 443, 420 cm⁻¹. HRMS (MALDI, DCTB): Found [M⁺] 637.164 for C₄₃H₂₈NOPS required 637.16237. m.p.: 185 °C

References

- (1) Baldo, M. A.; O'Brien, D. F.; You, Y.; Shoustikov, A.; Sibley, S.; Thompson, M. E.; Forrest, S. R., Highly efficient phosphorescent emission from organic electroluminescent devices. *Nature* **1998**, *395*, 151-154.
- (2) Hong, G.; Gan, X.; Leonhardt, C.; Zhang, Z.; Seibert, J.; Busch, J. M.; Bräse, S., A Brief History of OLEDs—Emitter Development and Industry Milestones. *Adv. Mater.* **2021**, *33*, 2005630.
- (3) Baldo, M. A.; O'Brien, D. F.; Thompson, M. E.; Forrest, S. R., Excitonic singlet-triplet ratio in a semiconducting organic thin film *Phys. Rev. B* **1999**, *60*, 14422-14448.
- (4) Baldo, M. A.; Adachi, C.; Forrest, S. R., Transient analysis of organic electrophosphorescence. II. Transient analysis of triplet-triplet annihilation. *Phys. Rev. B* **2000**, *62*, 10967-10977.
- (5) Adachi, C.; Baldo, M. A.; Thompson, M. E.; Forrest, S. R., Nearly 100% internal phosphorescence efficiency in an organic emitting device. *J. Appl. Phys.* **2001**, *90*, 5048-5051.
- (6) Poriel, C.; Rault-Berthelot, J., Blue Single-Layer Organic Light-Emitting Diodes Using Fluorescent Materials: A Molecular Design View Point. *Adv. Funct. Mat.* **2020**, *30*, 1910040.
- (7) Friend, R. H.; Gymer, R. W.; Holmes, A. B.; Burroughes, J. H.; Marks, R. N.; Taliani, C.; Bradley, D. D. C.; Dos Santos, D. A.; Bredas, J. L.; Lögdlund, M.; Salaneck, W. R., Electroluminescence in conjugated polymers. *Nature* **1999**, *397*, 121-128.
- (8) Sheats, J. R.; Antoniadis, H.; Hueschen, M.; Leonard, W.; Miller, J.; Moon, R.; Roitman, D.; Stocking, A., Organic Electroluminescent Devices. *Science* **1996**, *273*, 884-888.
- (9) Endo, A.; Ogasawara, M.; Takahashi, A.; Yokoyama, D.; Kato, Y.; Adachi, C., Thermally Activated Delayed Fluorescence from Sn⁴⁺–Porphyrin Complexes and Their Application to Organic Light Emitting Diodes — A Novel Mechanism for Electroluminescence. *Adv. Mater.* **2009**, *21*, 4802-4806.
- (10) Wong, M. Y.; Zysman-Colman, E., Purely Organic Thermally Activated Delayed Fluorescence Materials for Organic Light-Emitting Diodes. *Adv. Mater.* **2017**, *29*, 1605444.

- (11) Nakagawa, T.; Ku, S.-Y.; Wong, K.-T.; Adachi, C., Electroluminescence based on thermally activated delayed fluorescence generated by a spirobifluorene donor–acceptor structure *Chem. Commun.* **2012**, *48*, 9580-9582.
- (12) Zhang, Q.; Li, J.; Shizu, K.; Huang, S. Y.; Hirata, S.; Miyazaki, H.; Adachi, C., Design of Efficient Thermally Activated Delayed Fluorescence Materials for Pure Blue Organic Light Emitting Diodes. *J. Am. Chem. Soc.* **2012**, *134*, 14706-14709.
- (13) Xu, Q.-L.; Liang, X.; Zhang, S.; Jing, Y.-M.; Liu, X.; Lu, G.-Z.; Zheng, Y.-X.; Zuo, J.-L., Efficient OLEDs with low efficiency roll-off using iridium complexes possessing good electron mobility. *J. Mater. Chem. C* **2015**, *3*, 3694-3701.
- (14) Kim, M.; Lee, J. Y., Engineering of Interconnect Position of Bicarbazole for High External Quantum Efficiency in Green and Blue Phosphorescent Organic Light-Emitting Diodes. *ACS Appl. Mater. Interfaces* **2014**, *6*, 14874-14880.
- (15) Poriel, C.; Rault-Berthelot, J., Designing Host Materials for the Emissive Layer of Single-Layer Phosphorescent Organic Light-Emitting Diodes: Toward Simplified Organic Devices. *Adv. Funct. Mater.* **2021**, *31*, 2010547.
- (16) Yook, K. S.; Lee, J. Y., Organic Materials for Deep Blue Phosphorescent Organic Light-Emitting Diodes. *Adv. Mater.* **2012**, *24*, 3169-3190.
- (17) Wang, C.; Dong, H.; Hu, W.; Liu, Y.; Zhu, D., Semiconducting π -Conjugated Systems in Field-Effect Transistors: A Material Odyssey of Organic Electronics. *Chem. Rev.* **2012**, *112*, 2208-2267.
- (18) Poriel, C.; Rault-Berthelot, J.; Jiang, Z.-Q., Are pure hydrocarbons the future of host materials for blue phosphorescent organic light-emitting diodes? *Mater. Chem. Front.* **2022**, *6*, 1246-1252.
- (19) Wang, Y.; Yun, J. H.; Wang, L.; Lee, J. Y., High Triplet Energy Hosts for Blue Organic Light-Emitting Diodes. *Adv. Funct. Mater.* **2020**, *31*, 2008332.
- (20) Poriel, C.; Rault-Berthelot, J., Pure Hydrocarbons: An Efficient Molecular Design Strategy for the Next Generation of Host Materials for Phosphorescent Organic Light-Emitting Diodes. *Acc. Mater. Res.* **2022**, *3*, 379-390.
- (21) Kappaun, S.; Slugovc, C.; List, E. J. W., Phosphorescent Organic Light-Emitting Devices: Working Principle and Iridium Based Emitter Materials. *Int. J. Mol. Sci.* **2008**, *9*, 1527-1547.
- (22) Ingram, G.; Lu, Z.-H., Design principles for highly efficient organic light-emitting diodes. *J. Photonics Energy* **2014**, *4*, 040993.
- (23) Minaev, B.; Baryshnikov, G.; Agren, H., Principles of phosphorescent organic light emitting devices. *Phys. Chem. Chem. Phys.* **2014**, *16*, 1719-1758.
- (24) Helander, M. G.; Wang, Z. B.; Qiu, J.; Greiner, M. T.; Puzzo, D. P.; Liu, Z. W.; Lu, Z. H., Chlorinated Indium Tin Oxide Electrodes with High Work Function for Organic Device Compatibility. *Science* **2011**, *332*, 944-947.

- (25) Sasabe, H.; Seino, Y.; Kimura, M.; Kido, J., A m-Terphenyl-Modified Sulfone Derivative as a Host Material for High-Efficiency Blue and Green Phosphorescent OLEDs. *Chem. Mater.* **2012**, *24*, 1404-1406.
- (26) Li, W.; Li, J.; Liu, D.; Li, D.; Zhang, D., Dual n-type units including pyridine and diphenylphosphine oxide: effective design strategy of host materials for high-performance organic light-emitting diodes. *Chem. Sci.* **2016**, *7*, 6706-6714.
- (27) Lucas, F.; Ibraikulov, O. A.; Quinton, C.; Sicard, L.; Heiser, T.; Tondelier, D.; Geffroy, B.; Leclerc, N.; Rault-Berthelot, J.; Poriel, C., Spirophenylacridine-2,7-(diphenylphosphineoxide)-fluorene: A Bipolar Host for High-Efficiency Single-Layer Blue Phosphorescent Organic Light-Emitting Diodes. *Adv. Opt. Mater.* **2020**, *8*, 1901225.
- (28) Lucas, F.; Quinton, C.; Fall, S.; Heiser, T.; Tondelier, D.; Geffroy, B.; Leclerc, N.; Rault-Berthelot, J.; Poriel, C., Universal host materials for red, green and blue high-efficiency single-layer phosphorescent organic light-emitting diodes. *J. Mater. Chem. C* **2020**, *8*, 16354-16367.
- (29) Thiery, S.; Tondelier, D.; Geffroy, B.; Jeannin, O.; Rault-Berthelot, J.; Poriel, C., Modulation of the Physicochemical Properties of Donor-Spiro-Acceptor Derivatives through Donor Unit Planarisation: Phenylacridine versus Indoloacridine-New Hosts for Green and Blue Phosphorescent Organic Light-Emitting Diodes (PhOLEDs). *Chem. Eur. J.* **2016**, *22*, 10136-10149.
- (30) Romain, M.; Tondelier, D.; Geffroy, B.; Jeannin, O.; Jacques, E.; Rault-Berthelot, J.; Poriel, C., Donor/Acceptor Dihydroindeno[1,2-a]fluorene and Dihydroindeno[2,1-b]fluorene: Towards New Families of Organic Semiconductors. *Chem. Eur. J.* **2015**, *21*, 9426–9439,.
- (31) Romain, M.; Tondelier, D.; Jeannin, O.; Geffroy, B.; Rault-Berthelot, J.; Poriel, C., Properties modulation of organic semi-conductors based on a donor-spiro-acceptor (D-spiro-A) molecular design: new host materials for efficient sky-blue PhOLEDs. *J. Mater. Chem. C* **2015**, *3*, 9701-9714.
- (32) Zhu, X.-D.; Peng, C.-C.; Kong, F.-C.; Yang, S.-Y.; Li, H.-C.; Kumar, S.; Wang, T.-T.; Jiang, Z.-Q.; Liao, L.-S., Acceptor modulation for improving a spiro-type thermally activated delayed fluorescence emitter. *J. Mater. Chem. C* **2020**, *8*, 8579-8584.
- (33) Park, I. S.; Komiyama, H.; Yasuda, T., Pyrimidine-based twisted donor–acceptor delayed fluorescence molecules: a new universal platform for highly efficient blue electroluminescence. *Chem. Sci.* **2017**, *8*, 953-960.
- (34) Hempe, M.; Kukhta, N. A.; Danos, A.; Fox, M. A.; Batsanov, A. S.; Monkman, A. P.; Bryce, M. R., Vibrational Damping Reveals Vibronic Coupling in Thermally Activated Delayed Fluorescence Materials. *Chem. Mater.* **2021**, *33*, 3066-3080.
- (35) Romain, M.; Tondelier, D.; Jeannin, O.; Geffroy, B.; Rault-Berthelot, J.; Poriel, C., Properties modulation of organic semi-conductors based on a donor-spiro-acceptor (D-spiro-A) molecular design: new host materials for efficient sky-blue PhOLEDs. *J. Mater. Chem. C* **2015**, *3*, 97010-97014.

- (36) Romain, M.; Quinton, C.; Tondelier, D.; Geffroy, B.; Jeannin, O.; Rault-Berthelot, J.; Poriel, C., Thioxanthene and dioxothioxanthene dihydroindeno[2,1-*b*]fluorenes: synthesis, properties and applications in green and sky blue phosphorescent OLEDs. *J. Mater. Chem. C* **2016**, *4*, 1692-1703.
- (37) Poriel, C.; Rault-Berthelot, J.; Thiery, S.; Quinton, C.; Jeannin, O.; Biapo, U.; Geffroy, B.; Tondelier, D., 9H-Quinolino[3,2,1-*k*]phenothiazine: A New Electron-Rich Fragment for Organic Electronics. *Chem. Eur. J.* **2016**, *22*, 17930-17935.
- (38) Quinton, C.; Sicard, L.; Vanthuynne, N.; Jeannin, O.; Poriel, C., Confining Nitrogen Inversion to Yield Enantiopure Quinolino[3,2,1-*k*]Phenothiazine Derivatives. *Adv. Funct. Mater.* **2018**, *28*, 1803140-1803147.
- (39) Thiery, S.; Tondelier, D.; Geffroy, B.; Jacques, E.; Robin, M.; Métivier, R.; Jeannin, O.; Rault-Berthelot, J.; Poriel, C., Spirobifluorene-2,7-dicarbazole-4'-phosphine Oxide as Host for High-Performance Single-Layer Green Phosphorescent OLED Devices. *Org. Lett.* **2015**, *17*, 4682-4685.
- (40) Hsu, F.-M.; Chien, L.-J.; Chen, K.-T.; Li, Y.-Z.; Liu, S.-W., High morphology stability and ambipolar transporting host for use in blue phosphorescent single-layer organic light-emitting diodes. *Org. Electron.* **2014**, *15*, 3327-3332.
- (41) Lucas, F.; Tondelier, D.; Geffroy, B.; Heiser, T.; Ibraikulov, O. A.; Quinton, C.; Brouillac, C.; Leclerc, N.; Rault-Berthelot, J.; Poriel, C., Quinolophenothiazine as Electron Rich Fragment for RGB Single-Layer Phosphorescent Organic Light-Emitting Diodes. *Mater. Chem. Front.* **2021**, *5*, 8066-8077.
- (42) Yoshii, A.; Onaka, Y.; Ikemoto, K.; Izumi, T.; Sato, S.; Kita, H.; Taka, H.; Isobe, H., Acyclic, Linear Oligo-meta-phenylenes as Multipotent Base Materials for Highly Efficient Single-layer Organic Light-emitting Devices. *Chem. Asian J.* **2020**, *15*, 2181-2186.
- (43) Ma, X.; Liang, J.; Bai, F.; Ye, K.; Xu, J.; Zhu, D.; Bryce, M. R., New Mixed-C^N Ligand Tris-Cyclometalated Ir(III) Complexes for Highly-Efficient Green Organic Light-Emitting Diodes with Low Efficiency Roll-Off. *Eur. J. Inorg. Chem.* **2018**, *2018*, 4614-4621.
- (44) Wang, P.; Fan, S.; Liang, J.; Ying, L.; You, J.; Wang, S.; Li, X., Carbazole-diphenylimidazole based bipolar material and its application in blue, green and red single layer OLEDs by solution processing. *Dyes Pigm.* **2017**, *142*, 175-182.
- (45) Hung, W.-Y.; Wang, T.-C.; Chiu, H.-C.; Chen, H.-F.; Wong, K.-T., A spiro-configured ambipolar host material for impressively efficient single-layer green electrophosphorescent devices. *Phys. Chem. Chem. Phys.* **2010**, *12*, 10685-10687.
- (46) Thiery, S.; Tondelier, D.; Declairieux, C.; Geffroy, B.; Jeannin, O.; Métivier, R.; Rault-Berthelot, J.; Poriel, C., 4-Pyridyl-9,9'-spirobifluorenes as Host Materials for Green and Sky-Blue Phosphorescent OLEDs. *J. Phys. Chem. C* **2015**, *119*, 5790-5805.

- (47) Huang, B.; Jiang, W.; Tang, J.; Ban, X.; Zhu, R.; Xu, H.; Yang, W.; Sun, Y., A novel, bipolar host based on triazine for efficient solution-processed single-layer green phosphorescent organic light-emitting diodes. *Dyes Pigm.* **2014**, *101*, 9-14.
- (48) Zhang, Y.; Forrest, S. R., Triplet diffusion leads to triplet-triplet annihilation in organic phosphorescent emitters. *Chem. Phys. Lett.* **2013**, *590*, 106-110.
- (49) Kumar, M.; Pereira, L., Towards Highly Efficient TADF Yellow-Red OLEDs Fabricated by Solution Deposition Methods: Critical Influence of the Active Layer Morphology. *Nanomaterials* **2020**, *10*, 101.
- (50) Lee, S. S.; Loo, Y.-L., Structural Complexities in the Active Layers of Organic Electronics. *Annu. Rev. Chem. Biomol. Eng.* **2010**, *1*, 59-78.
- (51) Kim, S.-Y.; Jeong, W.-I.; Mayr, C.; Park, Y.-S.; Kim, K.-H.; Lee, J.-H.; Moon, C.-K.; Brütting, W.; Kim, J.-J., Organic Light-Emitting Diodes with 30% External Quantum Efficiency Based on a Horizontally Oriented Emitter. *Adv. Funct. Mater.* **2013**, *23*, 3896-3900.
- (52) Lu, C.-Y.; Jiao, M.; Lee, W.-K.; Chen, C.-Y.; Tsai, W.-L.; Lin, C.-Y.; Wu, C.-C., Achieving Above 60% External Quantum Efficiency in Organic Light-Emitting Devices Using ITO-Free Low-Index Transparent Electrode and Emitters with Preferential Horizontal Emitting Dipoles. *Adv. Funct. Mater.* **2016**, *26*, 3250-3258.
- (53) Wang, Q.; Lucas, F.; Quinton, C.; Qu, Y.-K.; Rault-Berthelot, J.; Jeannin, O.; Yang, S.-Y.; Kong, F.-C.; Kumar, S.; Liao, L.-S.; Poriel, C.; Jiang, Z.-Q., Evolution of pure hydrocarbon hosts: simpler structure, higher performance and universal application in RGB phosphorescent organic light-emitting diodes. *Chem. Sci.* **2020**, *11*, 4887-4894.
- (54) Köhler, A.; Bäessler, H., Triplet states in organic semiconductors. *Mat. Sci. Eng. C-Reports* **2009**, *66*, 71-109.
- (55) Steiner, F.; Vogelsang, J.; Lupton, J. M., Singlet-Triplet Annihilation Limits Exciton Yield in Poly(3-Hexylthiophene). *Phys. Rev. Lett.* **2014**, *112*, 137402.
- (56) Baldo, M. A.; Adachi, C.; Forrest, S. R., Transient analysis of organic electrophosphorescence. II. Transient analysis of triplet-triplet annihilation. *Phys. Rev. B* **2000**, *62*, 10967.
- (57) Wang, Y.-K.; Sun, Q.; Wu, S.-F.; Yuan, Y.; Li, Q.; Jiang, Z.-Q.; Fung, M.-K.; Liao, L.-S., Thermally Activated Delayed Fluorescence Material as Host with Novel Spiro-Based Skeleton for High Power Efficiency and Low Roll-Off Blue and White Phosphorescent Devices. *Adv. Funct. Mater.* **2016**, *26*, 7929-7936.
- (58) Wang, Q.; Tian, Q.-S.; Zhang, Y.-L.; Tang, X.; Liao, L.-S., High-efficiency organic light-emitting diodes with exciplex hosts. *J. Mater. Chem. C* **2019**, *7*, 11329-11360.
- (59) Su, S.-J.; Tanaka, D.; Li, Y.-J.; Sasabe, H.; Takeda, T.; Kido, J., Novel Four-Pyridylbenzene-Armed Biphenyls as Electron-Transport Materials for Phosphorescent OLEDs. *Org. Lett.* **2008**, *10*, 941-944.

- (60) Wang, Z. B.; Helander, M. G.; Qiu, J.; Puzzo, D. P.; Greiner, M. T.; Liu, Z. W.; Lu, Z. H., Highly simplified phosphorescent organic light emitting diode with >20% external quantum efficiency at >10,000cd/m². *App. Phys. Lett.* **2011**, *98*, 073310.
- (61) Ma, B.; Djurovich, P. I.; Garon, S.; Alleyne, B.; Thompson, M. E., Platinum Binuclear Complexes as Phosphorescent Dopants for Monochromatic and White Organic Light-Emitting Diodes. *Adv. Funct. Mater.* **2006**, *16*, 2438-2446.
- (62) Li, H.; Lam, T.-L.; Tan, X.; Dai, L.; Che, C.-M., 26-3: Invited Paper: High Performance and Long Device Lifetime Organic Light-emitting Diodes Using a Tetradentate Platinum (II) Emitter. *SID Symposium Digest of Technical Papers* **2021**, *52*, 328-331.
- (63) Fulmer, G. R.; Miller, A. J. M.; Sherden, N. H.; Gottlieb, H. E.; Nudelman, A.; Stoltz, B. M.; Bercaw, J. E.; Goldberg, K. I., NMR Chemical Shifts of Trace Impurities: Common Laboratory Solvents, Organics, and Gases in Deuterated Solvents Relevant to the Organometallic Chemist. *Organometallics* **2010**, *29*, 2176-2179.
- (64) Hohenberg, P.; Kohn, W., Inhomogeneous Electron Gas. *Phys. Rev.* **1964**, *136*, B864-B871.
- (65) Calais, J.-L., Density-functional theory of atoms and molecules. *Int. J. Quantum Chem.* **1993**, *47*, 101.
- (66) Becke, A. D., A new mixing of Hartree–Fock and local density-functional theories. *J. Chem. Phys.* **1993**, *98*, 1372-1377.
- (67) Becke, A. D., Density-functional thermochemistry. III. The role of exact exchange. *J. Chem. Phys.* **1993**, *98*, 5648-5652.
- (68) Becke, A. D., Density-functional exchange-energy approximation with correct asymptotic behavior. *Phys. Rev.* **1988**, *38*, 3098-3100.
- (69) Lee, C.; Yang, W.; Parr, R. G., Development of the Colle-Salvetti correlation-energy formula into a functional of the electron density. *Phys. Rev. B* **1988**, *37*, 785-789.
- (70) Frisch, M. J.; Trucks, G. W.; Schlegel, H. B.; Scuseria, G. E.; Robb, M. A.; Cheeseman, J. R.; Scalmani, G.; Barone, V.; Petersson, G. A.; Nakatsuji, H.; Li, X.; Caricato, M.; Marenich, A. V.; Bloino, J.; Janesko, B. G.; Gomperts, R.; Mennucci, B.; Hratchian, H. P.; Ortiz, J. V.; Izmaylov, A. F.; Sonnenberg, J. L.; Williams; Ding, F.; Lipparini, F.; Egidi, F.; Goings, J.; Peng, B.; Petrone, A.; Henderson, T.; Ranasinghe, D.; Zakrzewski, V. G.; Gao, J.; Rega, N.; Zheng, G.; Liang, W.; Hada, M.; Ehara, M.; Toyota, K.; Fukuda, R.; Hasegawa, J.; Ishida, M.; Nakajima, T.; Honda, Y.; Kitao, O.; Nakai, H.; Vreven, T.; Throssell, K.; Montgomery Jr., J. A.; Peralta, J. E.; Ogliaro, F.; Bearpark, M. J.; Heyd, J. J.; Brothers, E. N.; Kudin, K. N.; Staroverov, V. N.; Keith, T. A.; Kobayashi, R.; Normand, J.; Raghavachari, K.; Rendell, A. P.; Burant, J. C.; Iyengar, S. S.; Tomasi, J.; Cossi, M.; Millam, J. M.; Klene, M.; Adamo, C.; Cammi, R.; Ochterski, J. W.; Martin, R. L.; Morokuma, K.; Farkas, O.; Foresman, J. B.; Fox, D. J. *Gaussian 16 Rev. C.01*, Wallingford, CT, 2016.

